ELSEVIER

Surface Science 389 (1997) 366–374

surface science

Growth and surface alloying of Al on Au(111) at room temperature

B. Fischer, J.V. Barth *, A. Fricke, L. Nedelmann, K. Kern

Institut de Physique Expérimentale, Ecole Polytechnique Fédérale de Lausanne, CH-1015 Lausanne, Switzerland

Received 2 January 1997; accepted for publication 9 June 1997

Abstract

The initial stages of epitaxial growth of Al on Au(111) at room temperature have been investigated by scanning tunneling microscopy. In the submonolayer regime, large dendritic islands form. Their size distribution is found to be bimodal with the coexistence of a large area density of small and few large islands. The nucleation of second layer islands starts in advance of monolayer completion. Thicker films are rough. High-resolution data reveal that surface strain and intermixing of the two metals play a decisive role in the growth behavior: small quantities of adsorbed Al atoms strongly perturb the chevron reconstruction of clean Au(111) and a reconstruction pattern with hexagonal symmetry evolves for Al coverages exceeding ≈ 0.1 monolayers. This hexagonal domain wall phase consists of an intermixed Al–Au surface alloy layer with reduced atomic Al radii. © 1997 Elsevier Science B.V.

Keywords: Aluminum; Gold; Growth; Metallic films; Scanning tunneling microscopy; Single crystal surface; Surface alloying; Surface reconstruction

1. Introduction

Scanning tunneling microscopy (STM) has proven to be a valuable tool for the study of thin film growth on metal surfaces [1,2]. STM measurements provide crucial information on the atomic scale properties of the film structure and the growth kinetics. Local information is of particular importance when reconstructed substrates are studied, whose inherent defects can determine nucleation and growth of adlayers. This was demonstrated for instance for the growth of Ni and Co on Au(111), where the Au(111) surface reconstruction [3–6] stabilizes regular island patterns in the initial stages of thin film growth [7,8]. On the other hand, it has been demonstrated that the substrate reconstruction itself can be modified owing to the activity of adsorbed metals, which can drive both reconstruction phase transformations [9] or surface intermixing [10,11]. Processes of the latter kind have attracted much interest recently. In a number of cases, it has been shown that elements intermix at the surface, although they are immiscible in the bulk [12,13]. The driving force for the so-called surface alloying is the reduction of the strain energy related to the atomic size mismatch of the two constituents [14]. Moreover, in systems which are known to form stable bulk alloys, the kinetics of surface mixing turned out to be important, as the nucleation kinetics in the initial stages of growth is substan-

* Corresponding author. Fax: (+41) 21 6933604; e-mail: johannes.barth@ipe.dp.epfl.ch

PII S0039-6028(97)00451-2

tially altered with respect to systems growing phase separated [15].

In the following, we present an STM study of the growth and alloying of Al on Au(111). These metals are known to be miscible in the bulk. While the bulk lattice parameters of the two fcc (face centered cubic) metals are almost identical (4.08 and 4.04 Å for Au and Al, respectively), the surface free energy of Al (≈ 1200 mJ m^{-2}) is significantly lower than that of Au (≈ 1550 mJ m^{-2}). Based on the small lattice mismatch and the negative surface energy balance, pseudomorphic layer-by-layer growth might be expected from simple thermodynamics [16]. However, the Au(111) surface layer is uniaxially contracted along the close-packed lattice directions corresponding to a reduction of the surface lattice parameter of 4% along the contraction directions. Recently, it has been shown that epitaxial growth can be sensitively influenced by the strain field present in the surface layer of the substrate [17]. Indeed, helium diffraction measurements for the Al–Au(111) system revealed a complex temperature dependent growth behavior [18]. In addition, a symmetry change of the Au(111) reconstruction diffraction pattern was observed for Al deposition at temperatures exceeding 230 K, which was interpreted as Al-induced Au reconstruction [19]. It will be demonstrated that the complex nucleation and growth behavior above 230 K is related to Al intermixing into the topmost Au layer. Already minute quantities of incorporated Al strongly perturb the chevron reconstruction of the clean surface. The intermixing substantially affects the nucleation kinetics in the submonolayer coverage range resulting in an unusual bimodal island size distribution.

2. Experimental

The experiments were performed in an ultrahigh vacuum chamber (base pressure 3×10^{-10} torr), equipped with a variable temperature STM and standard facilities for sample preparation and characterization. The Au(111) single crystal was prepared by cycles of Ar^+ sputtering (1 μA cm^{-2}, 700 eV, 30 min at 300 K) and thermal annealing to 1000 K until no contaminations could be detected by Auger electron spectroscopy. STM measurements accordingly revealed the characteristic chevron pattern of the Au(111) reconstruction [5]. Aluminium atoms were evaporated from a Knudsen cell. During the deposition the Au sample was held at temperatures between 300 and 350 K. The Al coverage and flux were determined from the STM data recorded at low temperature (<200 K) [19]. Al coverages are given in terms of monolayers (ML), where 1 ML corresponds to 1 Al atom per Au atom of an unreconstructed (111) plane. For STM imaging, an electrochemically etched tungsten tip was used. The STM images, consisting typically of 512×512 data points, were acquired in the constant-current or differential mode (where the derivative dz/dx at constant current is recorded) with tunneling currents between 0.3 and 3 nA and voltages of 0.1–1.0 V. Constant current data are displayed in a top view gray-scale representation where darker areas correspond to lower levels. Data obtained in the differential mode appear as illuminated from the left in the graphical representation.

3. Results and discussion

The gross features of the initial stages of epitaxial growth of Al on the Au(111) surface at 310 K are illustrated by the STM data reproduced in Fig. 1. At $\theta_{Al} \approx 0.2$ ML (Fig. 1a), large islands with monolayer height (2.4 Å) and dendritic shape are found in the large terraces. The shape of the islands is related to a kinetic effect associated with anisotropic diffusion around island corners. As revealed in detail for dendritic growth of Ag islands on various fcc(111) substrates [17], atoms arriving at one-fold coordinated corner sites preferentially diffuse towards {100} steps thus promoting trigonal growth in the directions. The distances in between the islands are of the order of 1000 Å; hence, the atoms built in the islands must have diffused over several hundred Ångströms on the surface in the process of island formation. Dendritic growth of finger-like islands is similarly observed along the step edges of the Au substrate. With increasing coverages a bimodal island size distribution evolves. This is demonstrated by the

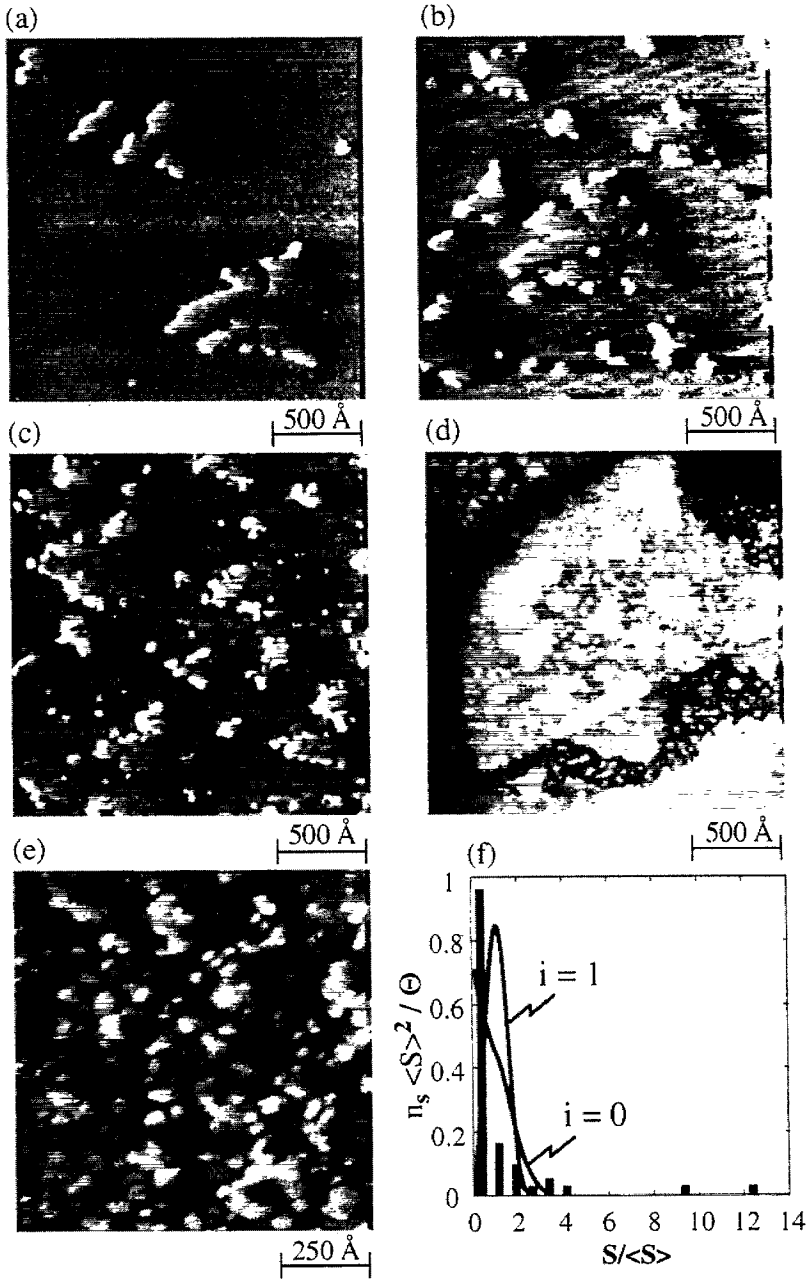

Fig. 1. Morphology of the Au(111) surface with Al deposited at 310 K (Al flux 0.05 ML min^{-1}): (a) $\theta_{Al} \approx 0.1$ ML; (b) $\theta_{Al} \approx 0.2$ ML; (c) $\theta_{Al} \approx 1.2$ ML; (d) $\theta_{Al} \approx 1.6$ ML; (e) $\theta_{Al} \approx 4.8$ ML; and (f) bimodal island size distribution at ≈ 0.2 ML coverage [S(⟨S⟩] island (mean island) size; n_S = island density, θ = coverage).

plot in Fig. 1f, where a statistical analysis of the island size distribution at about quarter monolayer coverage is reproduced. For this analysis, a series of STM images (5000×5000 Å^2 in size) have been evaluated quantitatively, revealing that a small number of very large islands coexist with many

small islands. In contrast to a regular nucleation and growth scenario on a homogenous surface, where a distribution for the scaled island density with a pronounced single maximum is expected [20–22], for the present system there is a clear deviation from this behavior. For comparison, calculated scaled island size distributions using the analytical expressions from Ref. [20] for a critical island size $i=0$ and $i=1$ are included in the plot in Fig. 1f (note that the curves for $i=2$ and $i=3$ are similar to $i=1$; for clarity, they are not shown). For the present system, however, two distinct classes of island sizes exist. For $S/\langle S\rangle<4$, the scaled island size distribution resembles the curve expected for the model case $i=0$. For intermediate and very large values, both calculated and experimental probabilities in the scaled island size distributions are zero. However, in sharp contrast to usual nucleation models, where the probability remains zero for all sizes with $S/\langle S\rangle$ exceeding 4, a second class of islands is clearly discernible in the experimental data for $S/\langle S\rangle$ between 9 and 12. The coexistence of these two classes of island sizes, i.e. the bimodal nature of the island size distribution, is understood as the result of a non-trivial growth mode prevailing for growth of Al on Au(111). The course of the scaled island size distributions of small islands signals that nucleation with a critical cluster size of 0 is of importance to the present system. This indicates the possibility of nucleation due to exchange processes between adsorbate and substrate atoms, similar to findings for the Fe–Cu(001) system [23].

Small second layer islands are formed already at $\theta_{Al}\approx 0.3$ ML on the largest islands of the first layer. For $\theta_{Al}\approx 1.0$ ML, percolation of the first layer islands and formation of larger second layer islands is observed. With increasing Al coverage, the completion of the first layer proceeds, while on the largest second layer islands there is already occupation of the third layer (Fig. 1c for $\theta_{Al}\approx 1.2$ ML). Once the first monolayer is completed, a density of second layer islands much higher than that of the first layer is observed, as is obvious from the tunneling image in Fig. 1d. This indicates that the mobility of the atoms on the first layer is much smaller than that on the clean substrate surface. For higher coverages, the density of islands on the surface shrinks again and films with simultaneous occupation of several Al layers are formed, as demonstrated by the STM image in Fig. 1e, where the surface morphology of an 4.8 ML Al film is reproduced.

The data reproduced in Fig. 1 demonstrate that the defects of the Au(111) chevron reconstruction do not simply act as nucleation centers for the deposited Al atoms, in which case regular island arrays would be formed. The unusual bimodal island distribution also indicates that the growth scenario for Al–Au(111) is dissimilar from heteroepitaxial growth on an unreconstructed metal substrate with trigonal symmetry. STM data on a smaller scale and with higher resolution demonstrate accordingly that the system is more complex and that the Au(111) substrate reconstruction reacts sensitively upon Al deposition. For coverages as low as a few percent (deposited at $T=$ 300–350 K), the Au(111) chevron structure is lifted and a highly distorted reconstruction domain pattern evolves. This is demonstrated by the tunneling image in Fig. 2 for $\theta_{Al}\approx 0.04$ ML. In the terraces, small islands are resolved [corrugation amplitude ≈ 2.4 Å, corresponding to the Au(111) monostep height]. The reconstruction deformation induced by the deposited Al on the substrate resembles patterns found on the clean surface in the vicinity of defects [5,24]. The basic features of the $(\sqrt{3}\times 22)$ domain structure are preserved: the light, pairwise corrugation lines (amplitude $\approx$ 0.2 Å) correspond to areas where surface atoms reside on bridge positions of the second layer, separating fcc and hcp (hexagonal close packed) stacking type domains. The fcc domains

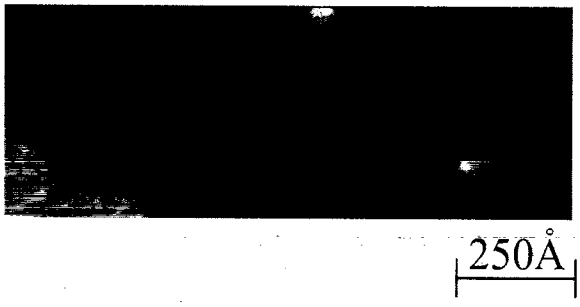

Fig. 2. Strongly perturbed Au(111) reconstruction pattern formed upon deposition of ≈ 0.04 ML Al at 300 K.

correspond to the wider areas between parallel running stripes [5]. It should be noted that the atoms in these areas do not reside on ideal fcc or hcp stacking type positions, as observed both for Au(111) [5] and isostructural features of the metastable Pt(111) reconstruction [25]. Rather, the surface layer is uniformly contracted along the close-packed directions and thus the observed fcc–hcp transitions are not to be understood in a strictly crystallographic sense.

For coverages exceeding ≈ 0.1 ML, the number of islands increases and a new poorly ordered surface reconstruction with hexagonal symmetry is formed. Upon Al adsorption at 300 K, this new reconstruction evolves exclusively in the terraces, whereas the islands exhibit a high defect density. For deposition at higher temperatures or upon gently annealing, however, the entire surface, including the islands, exhibits this reconstruction pattern, as illustrated by the STM image in Fig. 3a. (Note, that the islands formed upon annealing to 450 K are more compact than those in the data of islands formed at 300 K in Fig. 1 due to the increased surface atom mobilities at higher temperature. Because of the larger scales and the lower resolution of the low coverage STM data in Fig. 1, the existing reconstruction patterns are not resolved there.) This reconstruction closely resembles the Na-induced distorted hexagonal (DHEX) phase on Au(111) [9], which again is believed to be isostructural with the high temperature phase of the Au reconstruction [6]. Thus, the interpretation originally proposed for this phase is expected to be applicable also in the present case. The pattern formed is rationalized as a domain structure: the dark triangular areas are associated with fcc and hcp stacking domains and the light corrugation stripes with transition regions, where surface atoms reside on bridge type positions on the second layer and consequently are imaged higher (see inset in Fig. 3a). A schematic ball model illustrating the situation is reproduced in Fig. 3b. In the spots, where six stripes meet, surface atoms reside on or near top positions of the second layer and accordingly are imaged in the STM topographs with an increased corrugation amplitude [9,25]. As with the clean surface, the assignment of the stacking domains is qualitative, and it is likely that the contraction of the surface layer is rather uniform and not strictly localized in the corrugation lines.

The fact that the structural transformation exists on the entire surface rules out the possibility of an Al-induced Au reconstruction for the hexagonal pattern, for which pure Al islands with different structural features were expected. A phase separation of Al and Au within the surface layer corresponding to the observed features can be ruled out because of the wide Al coverage range for which the same hexagonal structure is observed [18] and the strong tendency towards alloy formation of the two metals. Consequently the surface must consist of an intermixed Al–Au surface layer which relaxes in the observed domain structure. For the Al–Au system, a rich variety of binary alloy phases exists [26–28] and thus the formation of a surface Al–Au alloy layer is not surprising. We could not obtain atomic resolution images, which would allow for an analysis of the atomic structure of the surface. However, with regard to the fact that Al and Au intermix easily for many stoichiometries in the bulk alloys, a homogeneous intermixing of Al and Au in the surface layer can be expected. This is in accordance with STM observations of Ag–Cu alloy thin films on Ru(0001), where a strain stabilized two dimensional alloy with a related domain structure was observed [29].

In accordance with the He diffraction results [18], we found that the Au(111) chevron reconstruction is preserved for deposition temperatures below 230 K [19]. The Al–Au DHEX evolves for $T > 230$ K, indicating that exchange of Al and Au atoms in the surface layer are possible well below room temperature. This finding is in agreement with results for the Pd on Au(111) system, where the onset of surface alloy formation was observed at temperatures exceeding 240 K [30], very similar to the present system. For the Na–Au(111) system, an even lower threshold temperature of ≈ 200 K for the formation of intermixed Na–Au surface layers was observed [11].

The Al–Au surface atom exchange processes are understood as the reason for the unusual bimodal island size distribution observed for submonolayer coverages upon Al deposition at 310 K. While our data do not allow for a quantitative analysis of

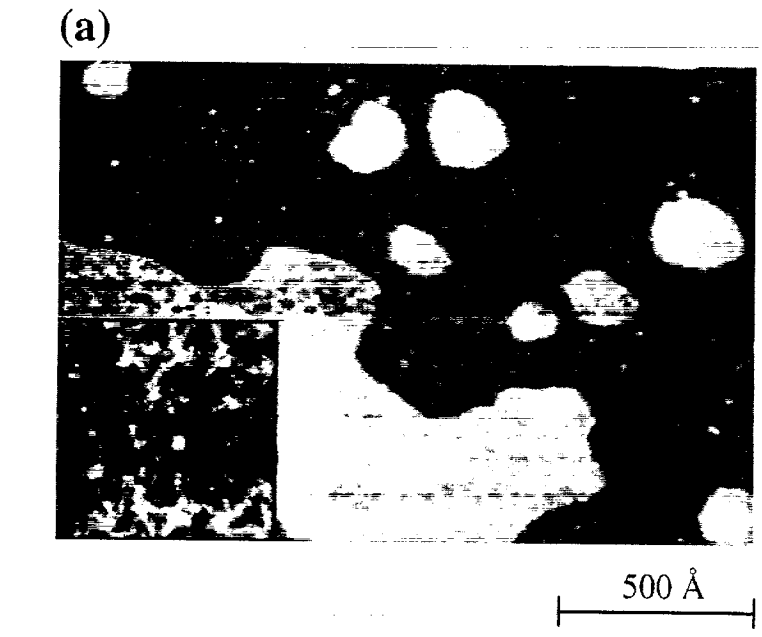

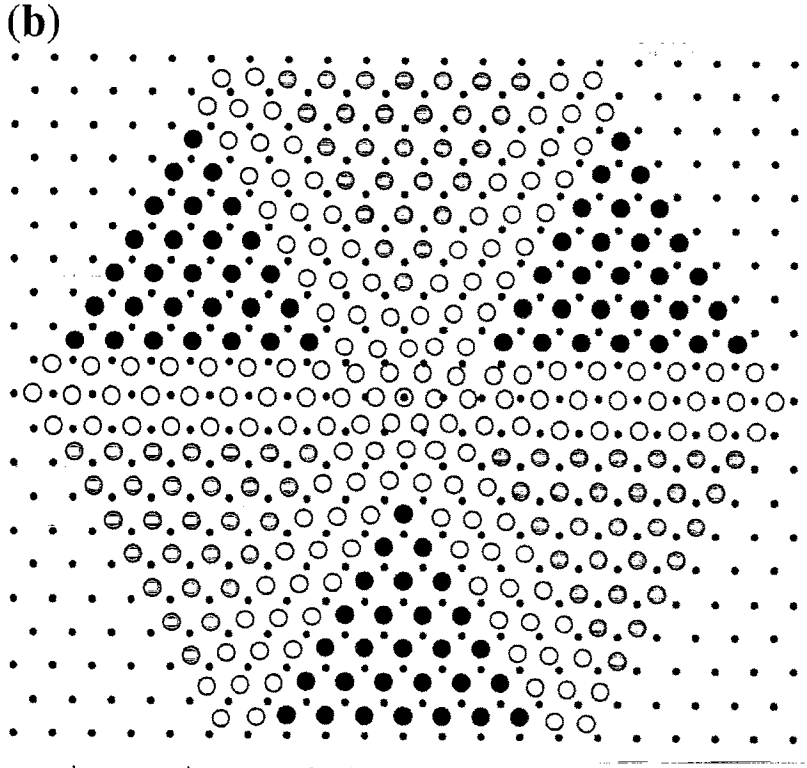

Fig. 3. (a) Distorted hexagonal reconstruction pattern of an intermixed Al–Au surface layer in terraces and on islands, formed upon deposition of ≈0.2 ML Al on Au(111) at 350 K and annealing to 450 K. Inset: 300 × 300 Å^2 blow-up of the reconstruction pattern. (b) Ball model for the Al–Au surface alloy domain structure. White (grey, dark) = surface Al or Au atoms close to bridge-top (hcp, fcc) type stacking positions. Black spots symbolize the Au atoms of the second layer.

the island formation process, the main features can be rationalized as follows. The coexistence of many small and few large islands indicate distinct processes for island nucleation with coverage or time dependent efficacy. Low temperature STM experiments revealed that the bimodal distribution occurs only for temperatures exceeding the critical temperature for surface atom exchange [19]. Hence, the large islands, which according to their size are formed initially, are associated with nucleation at sites where atom exchange can occur. STM experiments employing other deposits on Au(111) indicate that nucleation is initiated indeed by replacement of Au atoms at defect sites of the reconstruction [15]. We believe that such a mechanism is effective also in the present system and that the large islands nucleate in the early stages of deposition, where the density of monomers increases linearly with coverage ("transient regime" [31]). In the beginning of this regime, the mean free path of the atoms is large, which allows for rapid growth of these islands. However, with continuing deposition, on the one hand the monomer density increases implying a higher probability for adatom nucleation in the terraces without exchange processes, while on the other hand, the chevron reconstruction is heavily distorted once a small Al coverage has built up. This also might lead to a significant reduction of the mean free path of the atoms or an increased density of nucleation sites on the surface due to restructuring. The resemblance of the island distribution in Fig. 1f to the curve expected for $i=0$ suggests that due to the reconstruction changes, surface atom exchange processes leading to island nucleation might be facilitated [23]. A comprehensive analysis of the temperature-dependent growth behavior of Al on Au(111) will be presented elsewhere [19].

The periodicity of the Al–Au DHEX phase is 55–60 Å for an Al coverage of 0.1–0.2 ML, which is in good agreement with that derived from He diffraction data (52 Å for Al coverages of 0.1–0.5 ML deposited at 300 K [18]). From this periodicity, a contraction of the surface layer of 10% is inferred, i.e. the surface atom density amounts to 1.10 ML. This estimate is based on the model shown above (Fig. 3b), where the surface atom density is given by the simple expression: $[(l/a+1)/(l/a)]^2$ [a is the lattice parameter of a (111) Au bulk plane, 2.885 Å and l corresponds to the periodicity of the DHEX phase]. The He diffraction data demonstrate that for Al coverages exceeding 0.5 ML, the surface periodicity of the Au–Al DHEX further shrinks to reach a value as low as 30 Å close to monolayer coverage [18], which corresponds to an even higher surface atom density of ≈ 1.20 ML. The surface atom density of this phase is thus significantly higher than that of the Na-induced DHEX (1.06–1.09 ML [9]) or that of the isostructural Au(111) high-temperature phase (1.07 ML [6]). The formation of the latter structures was associated with a reduced coupling of the surface to the second Au layer which allows for a more uniform contraction of the surface Au layer [9]. The contraction of the Al–Au DHEX layer is thus unexpectedly large in view of the similar atomic radii of Al and Au. However, for Al–Au bulk binary alloys (and other binary alloys of Al with transition metals), it is well known that large negative deviations from the additivity of the atomic volumes exist, i.e. the Al atomic volume in certain alloys is considerably smaller than that in the fcc Al crystal [32,33]. The observed high contraction of the Al–Au surface alloy layer is thus rationalized as the two-dimensional analogue of the Al atom contraction in such binary bulk alloys. If we assume that the atomic radius of the Au atoms in the intermixed layer corresponds to that of the high temperature DHEX reconstruction phase, they occupy a surface area of $0.806\,a^2$ atom^{-1} [6]. With this value and the known contraction of the Al–Au surface layer, the average surface area occupied by the Al atoms for a coverage of 0.2 ML is estimated to $0.711\,a^2$ atom^{-1}, which is only 84% of the area of Al atoms in the (111) Al bulk plane, corresponding to a reduction of the Al atomic radii by $\approx 8\%$. For intermetallic fcc-type Al Au compounds, the Al atomic volume contraction amounts up to 10% (corresponding to a 3% radial contraction), indicating that the contractions in surface alloy formation can be stronger than those in the bulk. The driving force for the formation of the Al–Au DHEX structure is thus understood as a combination of: (1) surface strain; (2) energy gain by surface alloy formation; and (3) reduction in the

Al atomic diameter. The results demonstrate in particular, that changes of atom diameters must be considered when surface alloys of transition metals with Al (and presumably other free electron metals) are formed. Similar surface alloy domain structures are thus expected for Al–Ni, Al–Pd, Al–Pt and other systems, where also large metallurgical compressions for the respective bulk alloys exist [32,33]. The contraction of the Al atoms is associated with the fact that Al is a nearly free electron metal, which allows for effective charge transfer of aluminium atoms in the Au lattice. Analoguous atom contractions are typical for bulk alloy formation of the free electron alkali metals with Au and were observed in surface alloy formation of Na on Au(111) [11].

4. Conclusion

With the above findings of reconstruction changes and surface intermixing the growth of Al on Au(111) at $T=300$–350 K, whose gross features are presented in Fig. 1, can be described as follows. Initially, for Al coverages of the order of a few percent, the chevron reconstruction of clean Au(111) is heavily distorted and small islands are formed. For Al coverages exceeding ≈ 0.1 ML, intermixing of Al and Au at the surface definitely exists. Islands are formed in the terraces which must consist of both adsorbed Al atoms and Au atoms released in exchange processes in the terraces. Surface atom exchange processes also lead to an unusual bimodal island size distribution. The surface intermixing finally drives a phase transformation of the Au(111) chevron reconstruction to a poorly ordered surface alloy domain structure, which is of a similar type as the Na-induced or high-temperature DHEX phase of the Au(111) reconstruction. The surface layer of this phase is even more strongly contracted than that of the respective Au reconstructions, which is understood as a result of Al atom contraction in the surface alloy layer. The intermixing proceeds with increasing Al coverages until monolayer coverage is reached. For even higher coverages, the growth mode changes and a high density of islands is found (cf. Fig. 1d). The formation of these islands is associated with the termination of surface alloy formation and Al island nucleation at the defects of the Al–Au DHEX surface. For even thicker films, a reduced density of islands and growth of defect-free (111) Al films is accordingly observed where several surface Al layers are occupied simultaneously.

Acknowledgements

Fruitful discussions with H. Brune and financial support from the Alexander von Humboldt Stiftung (A.F.) and the Deutscher Akademischer Austauschdienst (L.N.) are gratefully acknowledged.

References

[1] C. Günther, S. Günther, E. Kopatzki, R.Q. Hwang, J. Schröder, J. Vrijmoeth, R.J. Behm, Ber. Bunsenges. Phys. Chem. 97 (1993) 522.
[2] H. Brune, K. Kern, in: D.A. King, D.P. Woodruff (Eds.), Physics and Chemistry of Solid Surfaces, vol. 8, Elsevier, Amsterdam, 1997.
[3] U. Harten, A.M. Lahee, J.P. Toennies, C. Wöll, Phys. Rev. Lett. 54 (1985) 2619.
[4] Y. K Takayanagi, K. Tanishiro, K. Yagi, K. Kobayashi, G. Honjo, Surf. Sci. 205 (1988) 637.
[5] J.V. Barth, H. Brune, G. Ertl, R.J. Behm, Phys. Rev. B 42 (1990) 9307.
[6] A.R. Sandy, S.G.J. Mochrie, D.M. Zehner, K.G. Huang, D. Gibbs, Phys. Rev. B 43 (1991) 4667.
[7] D.D. Chambliss, R.J. Wilson, S. Chiang, Phys. Rev. Lett. 66 (1991) 1721.
[8] B. Voigtländer, G. Meyer, N.A. Amer, Phys. Rev. B 44 (1991) 10354.
[9] J.V. Barth, R.J. Behm, G. Ertl, Surf. Sci. 302 (1994) L319 (1994); 312 (1994) L757 (erratum).
[10] E.I. Altman, R.J. Colton, Surf. Sci. 304 (1994) L400.
[11] J.V. Barth, R.J. Behm, G. Ertl, Surf. Sci. 341 (1995) 62.
[12] H. Röder, R. Schuster, H. Brune, K. Kern, Phys. Rev. Lett. 71 (1993) 2086.
[13] L.P. Nielsen, F. Basenbacher, I. Stensgaard, E. Lœgsgaard, C. Engdahl, P. Stoltze, K.W. Jacobsen, J. Nørskov, Phys. Rev. Lett. 71 (1993) 754.
[14] J. Tersoff, Phys. Rev. Lett. 74 (1995) 434.
[15] J.A. Meyer, I.D. Baikie, E. Kopatzkie, R.J. Behm, Surf. Sci. 365 (1996) L647.
[16] E. Bauer, Z. Kristallogr. 110 (1958) 372.
[17] H. Brune, K. Bromann, K. Kern, J. Jacobsen, P. Stoltze, K. Jacobsen, J. Nørskov, Surf. Sci. Lett. 349 (1996) L115.

[18] M.A. Krzyzowski, Ph.D. thesis, University of Bonn, 1995.
[19] B. Fischer, L. Nedelmann, H. Brune, J.V. Barth, K. Kern (to be published).
[20] J.G. Amar, F. Family, Phys. Rev. Lett. 74 (1995) 2066.
[21] J.W. Evans, M.C. Bartelt, Langmuir 12 (1996) 217.
[22] B. Müller, L. Nedelmann, B. Fischer, H. Brune, K. Kern, Phys. Rev. B 54 (1996) 17858.
[23] D.D. Chambliss, K.E. Johnson, Phys. Rev. B 50 (1994) 5012.
[24] Y. Hasegawa, P. Avouris, Science 258 (1992) 1763.
[25] M. Hohage, T. Micheley, G. Comsa, Surf. Sci. 337 (1995) 249.
[26] H. Büchler, K.-J. Range, J. Less-Common Metals 160 (1990) 143.
[27] J.L. Murray, H. Okamoto, T.B. Massalski, Bull. Alloy Phase Diag. 8 (1987) 20.
[28] H. Okamoto, J. Phase Equil. 12 (1991) 114.
[29] J.L. Stevens, R.Q. Hwang, Phys. Rev. Lett. 74 (1995) 2078.
[30] B.E. Koel, A. Sellidji, M.T. Paffet, Phys. Rev. B 46 (1992) 7846.
[31] J.W. Evans, M.C. Bartlet, J. Vacuum Sci. Technol. A 12 (1994) 1800.
[32] M. Ellner, K. Kolatschek, B. Predel, J. Less-Common Metals 170 (1991) 171.
[33] M. Ellner, B. Predel, in: J.H. Westbrook, R.L. Fleischer (Eds.), Intermetallic Compounds, vol. 1, Wiley, Chichester, 1994, p. 91.